Supplementary Online Materials for Maximov et al.,
"**Complexin Controls the Force Transfer from SNARE Complexes to Membranes in Fusion**"

EXPERIMENTAL PROCEDURES

Reagents and mice used. All toxins and ion channel blockers used for electrophysiological experiments were purchased from Tocris. Neurons were cultured as described (*S1, S2*)**.** The synaptobrevin-2 knockout mice were described previously (*S3*). All experiments were performed on cortical neurons cultured from wild-type mice (for complexin knockdown experiments) or from littermate wild-type and mutant offspring from heterozygous crossings of synaptobrevin-2 knockout mice.

Plasmid construction. The lentiviral constructs used in this paper were based on the pFUW vector (modified from pFUGW vector [*S4*]), a shuttle vector containing genes of interest and recombination arms for incorporating into the mammalian genome. The vector includes the HIV-1 flap sequence, the human polyubiquitin promoter-C, a multicloning site, and and WRE element (*S2*). The multicloning site contains six restriction sites XbaI, EcoRI, BstBI, NheI, BamHI and HpaI and is inserted into the BamHI and EcoRI site of pFUGW vectors by two oligonucleotide primers (5'-GATCGAATTCGAAGCTAGCGGATCCGTTAAC-3' and 5'-AATTGTTAACGGATCCGCT AGCTTCGAAGAATTC-3', respectively). To construct the complexin-1/2 shRNA lentivirus expression vector, we designed the oligonucleotides targeting identical sequences in the coding regions of mouse complexin-1 and complexin-2 (sense: 5'-GATCCCCCAGGACATGTTCA AGAAGTTTCAAGAGAACTTCTTGAACATGTCCTGTTTT TGGAAA-3'; antisense: 5'-AGCTTTTCCAAAAACAGGACATGTTCAAGAAGTTCTCTTGAAACTTCTTGAACATGTCC TGGGG-3). The oligonucleotides were annealed, phosphorylated and subcloned into Bgl II and Hind III sites of pSuper vector immediately downstream of the human H1 promoter. The cassette containing the H1 promoter and complexin-1 /2 oligonucleotide sequence was subsequently isolated by digestion with EcoR I and Cla I and subcloned into the EcoR I and BstBI sites located immediately upstream of the ubiquitin (Ub) promoter of the lentiviral shuttle vector. All rescue cDNA constructs with silent mutations at shRNA targeted sites were isolated by PCR and subcloned into BamH I and Bgl II sites located downstream of the ubiquitin promoter. The various

constructs contained the residues of rat complexin indicated (*S5*); the 4M mutant of complexin (*S6*) included the following amino acid substitutions: R48A/R59A/K69A/Y70A. All expression constructs were verified by sequencing.

Biochemical procedures. Various recombinant proteins were expressed and purified as GST fusion proteins that were eluted from glutathione-sepharose and further purified by ion-exchange column. Recombinant SNARE motifs and complexins were cleaved from GST by thrombin, and contaminants were removed by ion-exchange column. Mini-SNARE complexes were assembled from the SNARE motifs, purified, and tested for complexin- and synaptotagmin-binding and for temperature stability essentially as described (*S5*-*S8*). Mini-SNARE complexes were assembled by incubation of the 4 SNARE motifs in a 1:1:1:1 molar ratio overnight at 4 °C. SNARE complexes were purified on gel filtration and ion-exchange columns to remove unincorporated SNARE motifs. Mutant complexes were formed simply by replacing the wild-type synaptobrevin-2 SNARE motif with the mutant motif. The temperature stability of mini-SNARE complexes was tested by mixing the various mini-SNARE complexes with an identical volume of 2x SDS sample buffer, followed by a 5 min incubation at the indicated temperatures. Samples were cooled on ice and loaded onto an SDS-PAGE gel immediately. For protein affinity chromatography assay, GST-fusion proteins (3 μg of the complexin-1 or 30 μg of the synaptotagmin-1 C_2AB-domain GST fusion protein) were immobilized on glutathione-Sepharose, mini-SNARE complexes (with wild-type or mutant synaptobrevin-2) was added for binding, and samples were washed. In competition assay, additional recombinant complexin fragment 41-86 was added for replacement. SDS-PAGE, immunoblotting, and protein quantitations using ^{125}I-labeled secondary antibodies with phosphoImager detection to avoid the non-linearity of ECL were performed as described (*S8*).

Production of recombinant lentiviruses. Recombinant lentiviruses were produced by transfection of human embryonic kidney 293T cells with three plasmids, pFUW, pVSVg and pCMVΔ8.9, using FuGENE reagent (*S2, S4*). pVSVg and pCMVΔ8.9 encode the elements essential for packaging viral particles. Viruses were harvested 48 h after transfection by collecting the medium from transfected cells, and a 0.45 μm filter was used to remove cellular debris. Protein expression was tested in the transfected 293T cells to ensure viruses were working before they were applied to neurons. Neurons were infected with 250 μl of conditioned cell medium for each 24-well of high-

density neurons at 4 or 5 DIV, and the medium was exchanged to normal growth medium after 6 DIV, and kept until 14-18 DIV for biochemical and electrophysiological analyses.

Neuronal cultures and lentivirus infections. Primary cortical neurons were isolated from cortices of E18 or P1 pups of wild-type mice or synaptobrevin-2 deficient mice (*S1,S2*). The neurons were dissociated by trypsin digestion and plated on circle glass coverslips (Carolina Biological Supply) coated with Matrigel (Collaborative Biochemical Product, Inc). Neurons were maintained in MEM (Invitrogen) supplemented with B-27 (Invitrogen), glucose, transferin and Ara-C (Sigma). For all experiments, expression of rescue constructs was confirmed by immunoblotting and/or GFP fluorescence.

Immunocytochemistry and fluorescent imaging. Cultured wild-type neurons expressing complexin shRNA or a control transcript, or expressing various synaptobrevin constructs were analyzed by immunostaining and fluorescence imaging essentially as described (*S6*).

Electrophysiology. Analysis of synaptic transmission in cultured cortical neurons was performed as described (*S1*, *S2, S9*). Evoked synaptic responses were triggered by 1 ms current injections with a local extracellular stimulating electrode (FHC, Inc.), and were monitored from randomly selected nearby neurons by whole-cell recordings using a Multiclamp 700A amplifier (Axon Instruments, Inc.). The frequency, duration, and magnitude of extracellular stimulus were controlled with Model 2100 Isolated Pulse Stimulator (A-M Systems, Inc.). The whole-cell pipette solution contained 135 mM $CsCl_2$, 10 mM HEPES-NaOH pH 7.4, 1 mM EGTA, 1 mM Na-ATP 0.4 mM Na-GTP, and 1 mM QX-314. The resistance of filed pipettes varies between 3-5 mOhm. The bath solution contained 140 mM NaCl, 5 mM KCl, 2 mM or 10 mM CaCl2, 0.8 mM MgCl2, 10 mM HEPES-NaOH pH 7.4, and 10 mM glucose. EPSCs and IPSCs were separated pharmacologically by addition to the bath solution of 0.1 mM picrotoxin or 0.05 mM AP-5 and 0.01 mM CNQX, respectively. mEPSCs and mIPSCs were monitored under the same conditions in the presence of 1 μM tetrodotoxin. The currents were sampled at 10 kHz and analyzed offline using pClamp9 (Axon Instruments, Inc.) and Origin7 (Origin Lab) software. To construct cumulative charge histograms, responses recorded from each neuron were integrated over 0.8 s for single action potential stimulation and over 5 s for stimulus trains. The time constants of single evoked responses were determined by double exponential fits ($y = y0 + A1*\exp(-(x-x0)/t1) + A2*\exp(-(x-x0)/t2)$). For

analysis of release triggered by trains of action potentials, the time period from the beginning of the first stimulus to 100 ms after the last stimulus was defined as the period of "train release" (TR). The remaining current (the current observed after 100 ms after the last stimulus) was defined as delayed release (DR). The total charge transfer was defined as an average of sums of TR and DR. Miniature postsynaptic currents were captured and analyzed using pClamp template search function. Measurements of EPSCs at different extracellular Ca^{2+}-concentrations to evaluate the Ca^{2+}-responsiveness of synaptic transmission in complexin knockdown neurons was performed as described (*S2*). For representation purposes, the stimulus artifacts were removed by filtering the current traces at 40-50 Hz.

Statistical analyses. All data are presented as means ± SEMs. p values were calculated using the ANOVA test and presented as follows: ***$p < 0.001$; **$p < 0.01$; *$p < 0.05$. In complexin-1 /2 shRNA knock-down experiments, all groups were compared for control GFP-expressing neurons. In synaptobrevin-2 rescue experiments, all groups were compared to neurons expressing Syb-2 WT. Numerical values for all electrophysiology results are listed in Table S1.

SUPPLEMENTARY TEXT

Effectiveness and effects of shRNA-mediated knockdown of complexins. Although the shRNA we used is directed to an RNA sequence that is 100% identical between mouse complexin-1 and -2, the knockdown is more efficient for complexin-1 than for complexin-2 (Fig. S1). Co-expression of wild-type complexin-1 with the complexin shRNA restored normal levels of complexin-1, whereas the apparent levels of 4M-mutant complexin-1 were lower, possibly because the mutation partially ablates the antibody epitope, and/or because the mutation may destabilize the protein (Fig. S1). In electrophysiological experiments, the complexin shRNA had little effect on inhibitory synaptic transmission, possibly because complexin-2 might be expressed at higher levels in inhibitory synapses and was suppressed to a lower degree than complexin-1 by the shRNA (Fig. S1). Different from previous observations in complexin-deficient autapses (*S10*, *S11*), the deficit in fast synaptic transmission in complexin knock-down neurons, or in knock-down neurons rescued with N-terminally truncated complexin (Cpx^{41-134}), could not be restored by elevation of extracellular Ca^{2+} (Fig. S3). In other words, the decrease in evoked neurotransmitter release induced by a loss of complexin is not due to a shift in the Ca^{2+}-sensitivity of release, but alter all of the synchronous Ca^{2+}-triggered release process.

Characterization of the effects of the synaptobrevin mutations on SNARE-complex formation and SNARE-complex binding to complexin and synaptotagmin-1. We introduced six mutations into synaptobrevin-2:

1. A mutation into the SNARE-motif that is predicted based on the crystal structure (*S7*) to selectively impair only complexin binding but not SNARE complex formation (the 3A-mutation = alanine substitutions of V^{50}, L^{54}, and D^{57}; Fig. S6A)
2. A second mutation into the SNARE-motif that is predicted based on the crystal structure (*S7*) to alter only SNARE-complex formation (the 3'A-mutation = alanine substitutions of D^{64}, D^{65}, and D^{68}; Fig. S6A). Note that this mutation was only analyzed biochemically but not functionally.
3. A third mutation into the SNARE-motif that consists of the combination of the 3A and 3'A mutations (see 1. and 2.), and is predicted based on the crystal structure (*S7*) to alter both complexin binding and SNARE-complex formation (the 6A-mutation = alanine substitutions of V^{50}, L^{54}, D^{57}, D^{64}, D^{65}, and D^{68}; Fig. S6A).
4. A mutation into the linker connecting the SNARE motif to the transmembrane region (TMR), just outside of the TMR, that should have no effect on SNARE-complex formation (the WA-mutation = alanine substitutions of W^{89} and W^{90}; Fig. S6A) because the corresponding sequence is several residues away from the SNARE-complex forming SNARE motif.
5. Two additional mutations into the same linker adjacent to the WA-mutation (the 85- and 86-mutations = alanine substitutsions of K^{85} and R^{86}, or of R^{86} and K^{87}; Fig. S6A). Note that these mutations were only analyzed electrophysiologically but not biochemically because their location did not suggest a biochemical effect on SNARE-complex formation, and because, different from the WA mutation, these mutations caused no detectable change in neurotransmitter release and synaptobrevin function.

We analyzed the 3A-, 3'A-, 6A-, and WA-mutations biochemically, but not the 85- and 86-mutation because they exhibited no electrophysiological phenotype. We analyzed all of these mutants except for the 3'A-mutant electrophysiologically (Figs. 1-3 and S14). The 3'A-mutant was not analyzed electrophysiologically because it exhibits a selective impairment in SNARE-complex assembly but

not in complexin binding, and would thus not have provided additional information beyond the 3A- and 6A-mutants. For the biochemical anlayses, we assembled recombinant mini-SNARE complexes containing wild-type, 3A-, 3'A-, 6A-, or WA-mutant synaptobrevin-2, and tested the stability of these SNARE complexes using heat denaturation assays, and the binding of these SNARE complexes to complexin and synaptotagmin-1 using GST-pulldowns (Figs. S6 and S7). When exposed to increasing temperatures, SNARE complexes containing 3'A- and 6A-mutant synaptobrevin denatured at lower temperatures than control SNARE complexes, whereas SNARE complexes containing 3A- or WA-mutant synaptobrevin denatured at the same temperature as control SNARE complexes (Fig. S7). This result suggests that the 3'A- and 6A-mutations but not the 3A- or WA-mutations impair SNARE-complex stability. The 3A- and the 6A-mutations, however, abolished complexin binding, whereas the 3'A- and WA-mutations had no effect on complexin-binding to SNARE complexes. Moreover, the 3A- and WA-mutations had no effect on synaptotagmin-1 binding, whereas the 6A-mutation also impaired this activity (Figs. 1C and 1D). The 3A- and 6A-mutations thus provide a tool to differentiate between the functional importance of SNARE-complex stability vs. SNARE-complex binding to complexin. The WA-mutation, in contrast, has no apparent effect on the biochemical properties of synaptobrevin as a SNARE protein.

Differences between our results and those observed previously with other approaches. Many of our findings in complexin-deficient synapses resemble those described previously for synapses from complexin knockout mice (*S10*, *S11*). Two significant differences were found, however: different from the knockout analysis, we detected a large increase in mini-frequency (Fig. 1); on the other hand, we did not observe any rescue of the complexin loss-of-function phenotype by high Ca^{2+}-concentrations (Fig. S3).

These differences could be due to either developmental compensation in the knockout that is absent in the acute shRNA-mediated knockdown, or to the differences in preparations used (autapses vs. synapses between neurons in high-density cultures). Significant evidence favors the latter explanation. A similar difference between autapses and synapes between neurons was observed previously in the analysis of synaptotagmin-1 deficient synapses – especially, the same difference in spontaneous release as detected there, despite the fact that both analyses employed constitutive knockout mice (*S8*, *S9*, *S12*). Thus, a developmental compensation appears an unlikely explanation.

It is remarkable that the complexin-deficiency phenotype resembles the synaptotagmin-deficiency phenotype almost completely, as it exhibits exactly the same features, even an inability to rescue the phenotype by high Ca^{2+}-concentrations.

Conversely, our results differ dramatically from those obtained in Drosophila and in in vitro fusion assays in that in these preparations the positive function of complexin as an activator of fusion was only marginally apparent (*S13*-*S15*). The reason for this discrepancy is likely to differ for the in vitro fusion assays and the Drosophila experiments. In the in vitro fusion assays, under standard conditions SNAREs by themselves are sufficient to perform fusion, and an enhancing activity of complexin would simply not have been observed. This is different from the in vivo situation where SNAREs alone are not sufficient (*S16*). In the Drosophila experiments, neuromuscular junctions were analyzed. Previous studies showed that genetic loss-of-function mutations in exocytosis often lead to expansion of the neuromuscular junction (*S17*). Thus, a loss-of-function in exocytosis may have simply been overlooked, especially since a small such loss-of-function was observed.

Our findings also prompt a reinterpretation of studies in which the linker between the SNARE motif and transmembrane region was altered. Increases in the size of the linker in synaptobrevin/VAMP impair synaptic vesicle fusion in synapses (*S18*). In addition to this phenotype, in chromaffin cells such insertions cause a deceleration of fusion, a finding that, as shown here, may be due to a change in complexin function and not directly related to SNARE function itself (*S19*).

SUPPLEMENTARY FIGURE LEGENDS

Supplementary Fig. S1

Complexin knockdown by shRNAs expressed in neurons with recombinant lentiviruses.

A, Diagram of the lentiviral vectors encoding the shRNA targeting both complexin-1 and -2 (top), and the domain structure of complexin (middle). The sequences of the central SNARE-binding α-helix from wild-type (WT) and mutant complexin-1 (4M, containing the following amino acid substitutions: R48A/R59A/K69A/Y70A) are shown at the bottom. In the lentiviral vectors, shRNA expression is driven by the human H1 promoter, and cDNA expression for rescues is driven by the ubiquitin promoter (Ub). The complexin diagram displays the location of the N-terminal (blue) and C-terminal sequences (white), of the accessory N-terminal α-helix (yellow), and of the central SNARE-binding α-helix (red). In the sequences of 4M-mutant complexin, mutant residues ($R^{48}/R^{59}/K^{69}/Y^{70}$) are depicted in red.

B, Immunoblot analysis of complexin knockdown. Protein extracts from cultured cortical neurons infected with lentiviruses were analyzed by immunoblotting with the indicated antibodies, using either HRP-tagged secondary antibodies and visualization by enhanced chemiluminescence (blot shown), or ^{125}I-labeled secondary antibodies and phosphoImager quantitation (panels C and D). For the analysis, wild-type mouse neurons were infected with lentivirus expressing GFP only (control), or lentivirus transcribing an shRNA that targets both complexin-1 and -2 (Cpx-1/2 shRNA); the same lentivirus additionally expresses either GFP, wild-type rat complexin-1 that is not targeted by the shRNA (Cpx^{1-134}), or mutant rat complexin-1 with inactivated SNARE-binding sites (Cpx^{1-134} 4M). Note that 4M-mutant complexin-1 appears to be expressed less well than wild-type complexin-1, possibly because alanine substitutions alter antibody reactivity.

C and **D,** Quantitation of complexin protein levels in neurons expressing complexin-1/2 shRNA in the multiple experiments similar to that described in panel B. Protein expression levels were determined by quantitative immunoblotting with corresponding primary and ^{125}I -labeled secondary antibodies. Panel C depicts the quantitation results for complexin-1 and -2, and panel D the quantitation results for several synaptic control proteins as indicated. Data shown are means ± SEMs (* = $p<0.05$; ** = $p<0.01$ compared to control per two-way ANOVA).

Supplementary Fig. S2

Complexin knockdown does not alter synapse density

A and **B,** Representative images (A) and summary graphs of quantitations obtained in multiple independent experiments (B). Cortical neurons were infected with lentivirus expressing GFP only (control) or the complexin shRNA together with GFP (Complexin shRNA). Neurons were fixed, stained for MAP2 to visualize dendrites and for synapsin to visualize nerve terminals, and analyzed quantitatively using the metamorph program suite to measure synapse numbers (quantified as the number of synapsin-positive boutons per dendritic length) and synapse size (measured as the intensity of the synapsin signal). The data in B depitc values determined in three independent experiments, with the number of neurons analyzed shown in the bar diagrams. shRNA samples are not significantly different from controls by a two-way ANOVA analysis).

Supplementary Fig. S3

Ca^{2+}-sensitivity of evoked release in complexin-deficient neurons.

Cultured cotrical neurons were infected with control lentivirus or lentivirus expressing shRNA alone (shRNA) or shRNA with either the full-length complexin rescue (Cpx^{1-134}) or the truncated complexin rescue (Cpx^{1-134}). Synaptic responses evoked by isolated action potentials were measured as a function of the extracellular Ca^{2+}-concentration. Superimposed representative traces are shown on the left, and a summary graph (means ± SEMs; n = 5-25 neurons/group in 3 independent experiments) on the right. Note that the responses in neurons expressing the shRNA without rescue, or the shRNA with rescue with N-terminally truncated complexin lacking residues 1-40 were significantly different from the control neurons or neurons expressing the shRNA with rescue by full-length complexin at the $p<0.001$ level as analyzed by two-way ANOVA). This experiment establishes that the complexin knockdown does not simply decrease the Ca^{2+}-affinity for fusion, but affects all fast Ca^{2+}-induced fusion.

Supplementary Fig. S4

A 10 Hz stimulus train induces normal total release in complexin-deficient neurons

A and **B,** Representative traces (A; scale bars apply to all traces) and mean total charge transfer (B) of EPSCs triggered by a 10 Hz train of 10 action potentials in neurons infected with control or complexin knockdown lentivirus as described in Figure S1A.

C and **D,** Plots of the cumulative charge transfer during the 10 Hz action potential train as a function of time (TR = period of train release; DR = delayed release; C), and relative contribution of delayed release to the total synaptic charge transfer in neurons infected with the various lentiviruses (D)..

Data in B and D are means ± SEMs; statistical significance was evaluated by ANOVA in comparison to control neurons: *** = $p<0.001$; numbers of analyzed neurons are shown in Fig. 1.

Supplementary Fig. S5

Schematic diagram of truncated complexins (A), and sufficiency of the complexin SNARE-binding α-helix for displacing synaptotagmin from SNARE complexes.

A, Structures of truncated complexins used for rescue analysis. Note that complexins contain two α-helices: an N-terminal accessory α-helix (residues 28-47), and a central SNARE-binding α-helix (residues 48-70).

B, The central SNARE-binding α-helix of complexin is sufficient for displacement of synaptotagmin-1 from SNARE complexes. Recombinant mini-SNARE complexes were assembled with wild-type syntaxin-1, SNAP-25 and synaptobrevin-2. Binding of SNARE complexes to GST-fusion protein of the C_2AB-domain fragment of synaptotagmin-1 was monitored in the presence of increasing concentrations of a complexin fragment consisting only of the central α-helix with flanking sequences (Cpx^{41-86}). Binding was performed in the absence or presence of 1 mM free Ca^{2+}. Images show a Coomassie blue-stained gel of proteins bound to the immobilized GST-synaptotagmin fusion protein; data are from representative experiments that were repeated al least three times.

Supplementary Fig. S6

Synaptobrevin mutations: overview and effect on SNARE complex formation

A, Location and sequence of all of synaptobrevin mutations analyzed in the present study. Two types of point mutations were analyzed: Mutations in the SNARE motif (left sequences below the domain structure of synaptobrevin), and mutations in the linker sequence connecting the SNARE motif to the transmembrane region (TM). In the sequences at the bottom, mutations are depicted in red.

B and **C**, Temperature stability of mini-SNARE complexes formed with the recombinant SNARE motifs from syntaxin-1 and SNAP-25 and wild-type (Syb2 WT) or mutant synaptobrevin-2 (Syb2 3A, 3'A, 6A and WA; note that the 85 and 86 mutants were not analyzed biochemically because of a lack of functional phenotype, and that the 3'A mutant was not analyzed electrophysiologically because it only exhibits a change in SNARE complex formation). Panel B depicts coomassie blue-stained SDS gels of the assembled complexes incubated at the indicated temperatures, and panel C quantitations of the temperature stability as determined in 3 independent experiments, with SNARE complexes measured by scanning of Coomassie-stained gels.

Supplementary Fig. S7

Effect of various synaptobrevin mutations on the binding of mini-SNARE complexes containing these synaptobrevins to GST-fusion proteins of complexin (GST-Cpx; panel A) or of synaptotagmin-1 (GST-Syt, panel B)

SNARE complexes containing the various mutants of synaptobrevin-2 were assembled, and bound to the GST-fusion proteins of full-length complexin-1 (GST-Cpx; A) or of the two C2-domains of synaptotagmin-1 (GST-Syt; B). GST-fusion proteins were immobilized on gluthatione-Sepharose. Data shown represent Coomassie-stained SDS-gels from experiments that were independently performed at least three times. GST-Syt binding was carried out in the absence and presence of 1 mM Ca^{2+} as indicated.

Supplementary Fig. S8

mEPSC and mIPSC amplitudes in synaptobrevin-2 KO neurons rescued with wild-type and mutant synaptobrevins

Bar diagrams depict means ± SEMs of the mini amplitudes (see Fig. 2A-2D for details; there is no statistically significant difference between the various samples as analyzed by ANOVA).

Supplementary Fig. S9

Scaled superimposed traces of IPSCs triggered by isolated action potentials in synaptobrevin-2 KO neurons expressing wild-type, WA-mutant, or 3A-mutant synaptobrevin-2

Data shown are representative traces that are typical for the responses observed to illustrate the asynchronous nature of the mutant responses. See Figs. 2 and 3 for quantitations of synaptic responses.

Supplementary Fig. S10

Synaptic charges transferred by IPSCs induced by 10 Hz stimulus trains for 1 s in synaptobrevin-2 KO neurons expressing GFP (control)**, or wild-type** (Syb2 WT)**, 3A-mutant** (Syb2 3A)**, or 6A-mutant synaptobrevin-2** (Syb2 6A).

A, Total synaptic charge transfer induced by the entire stimulus train, including delayed release.

B, Charge transfer only during the stimulus train

C, Charge transfer only during the delayed release phase

Data shown are means ± SEMs (* = $p<0.05$; *** = $p<0.001$ compared to wild-type synaptobrevin per ANOVA).

Supplementary Fig. S11

WA-mutant synaptobrevin-2 is correctly targeted to synaptic vesicles

Panels depict fluorescence images of cortical neurons that express either Venus alone (Venus), or Venus fusion proteins of wild-type synaptobrevin-2 (Syb2-Venus) or of WA-mutant synaptobrevin-2 (Syb2WA-Venus) Cortical neurons cultured from newborn animals were infected at 4 days in vitro (DIV) with lentiviruses expressing the respective proteins. Triple imaging for the expressed Venus-fusion proteins and for synapsin and MAP2 labeled by immunofluorescence was performed at 14 DIV. Confocal images were collected using Zeiss LSM 510. Mono-clonal Map2 antibody (M1406, Sigma; blue; left panels) and polyclonal synapsin antibody (E028; red) were used for immunofluorescence labeling; mVenus (Green) signals are from recombinant proteins introduced by lentiviruses. The right panels display merged images. Arrow heads indicate co-localization of synaptobrevin-Venus fusion proteins with endogenous synapsins (scale bar= 10 μm).

Supplementary Fig. S12

mEPSC and mIPSC amplitudes in synaptobrevin-2 KO neurons rescued with wild-type and WA-mutant synaptobrevin

Bar diagrams depict means ± SEMs of the mini amplitudes (see Fig. 3 for details; there is no statistically significant difference between the various samples as analyzed by ANOVA).

Supplementary Fig. S13

Synaptic charges transferred by IPSCs induced by 10 Hz stimulus trains for 1 s in synaptobrevin-2 KO neurons expressing GFP (control)**, wild-type** (Syb2 WT) **WA-mutant synaptobrevin-2** (Syb2 WA).

A, total synaptic charge transfer during the stimulus train

B, synaptic charge transfer only during the stimulus train

C, synaptic charge transfer during the delayed releaes phase

Data shown are means ± SEMs (*** = $p<0.001$ compared to wild-type synaptobrevin per ANOVA; n=3 independent cultures).

Supplementary Fig. S14

Analysis of synaptic transmission in synaptobrevin-2 KO neurons infected with lentiviruses expressing GFP only (control), wild-type synaptobrevin-2 (Syb2 WT), or 85- or 86-mutant synaptobrevin-2 carrying the K85A/R86A (Syb2 85) or the R86A/K87A substitutions (Syb2 86; see Fig. S7 for a description of these mutants).

A-C, properties of spontaneous excitatory postsynaptic currents. Data show representative traces (A) and summary graphs of the frequency (B) and amplitudes (C) of mEPSCs monitored in the presence of tetrodotoxin and GABA receptor blockers.

D and **E,** excitatory postsynaptic currents evoked by isolated action potentials. Data show representative traces (D) and summary graphs of the amplitudes (E) of EPSCs evoked by focal stimulation of action potentials at 0.1 Hz.

F-H, excitatory postsynaptic currents evoked by a 10 Hz – 1 s stimulus train. Data show representative traces (F) and summary graphs of the total synaptic charge transfer (G) or only the synaptic charge transfer during delayed release (H).

I-K, spontaneous inhibitory postsynaptic currents. Data show representative traces (I) and summary graphs of the frequency (J) and amplitudes (K) of mIPSCs monitored in the presence of tetrodotoxin and glutamate-receptor blockers.

L and **M,** inhibitory postsynaptic currents evoked by isolated action potentials, induced by focal stimulation at 0.1 Hz. Data show representative traces (L) and summary graphs of the amplitudes (M) of IPSCs.

N-P, inhibitory postsynaptic currents evoked by a 10 Hz – 1 s stimulus train. Data show representative traces (N) and summary graphs of the total synaptic charge transfer (O) or only the synaptic charge transfer during delayed release (P).

In A, D, F, I, and L, scale bars apply to all traces in the series; all bar diagrams depict means ± SEMs; statistical significance was evaluated by ANOVA in comparison to wild-type synapbrevin-2: *** = $p<0.001$; total number of analyzed neurons in 3 independent cultures are shown in the bars.

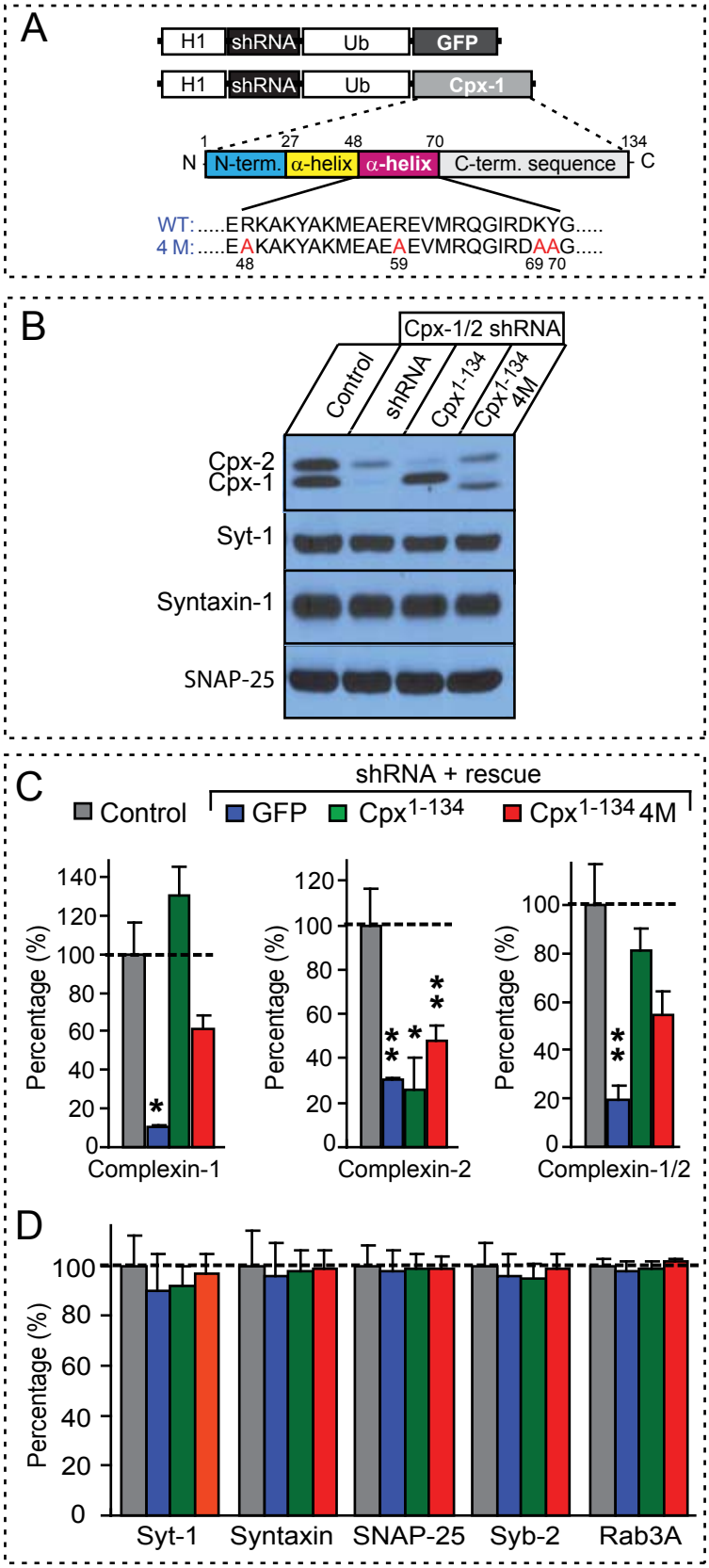

Suppl. Fig. S1
Maximov et al.

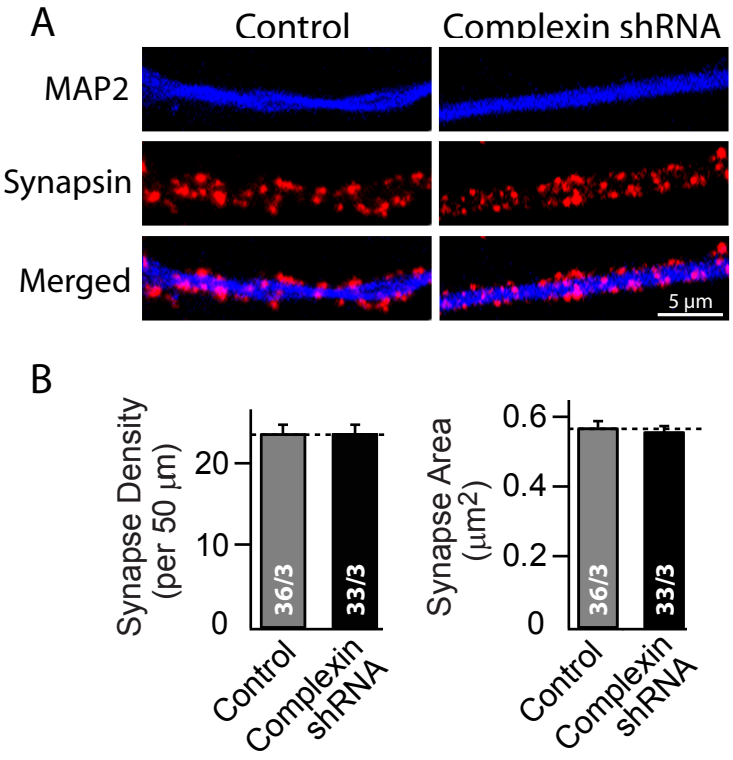

Suppl. Fig. S2
Maximov et al.

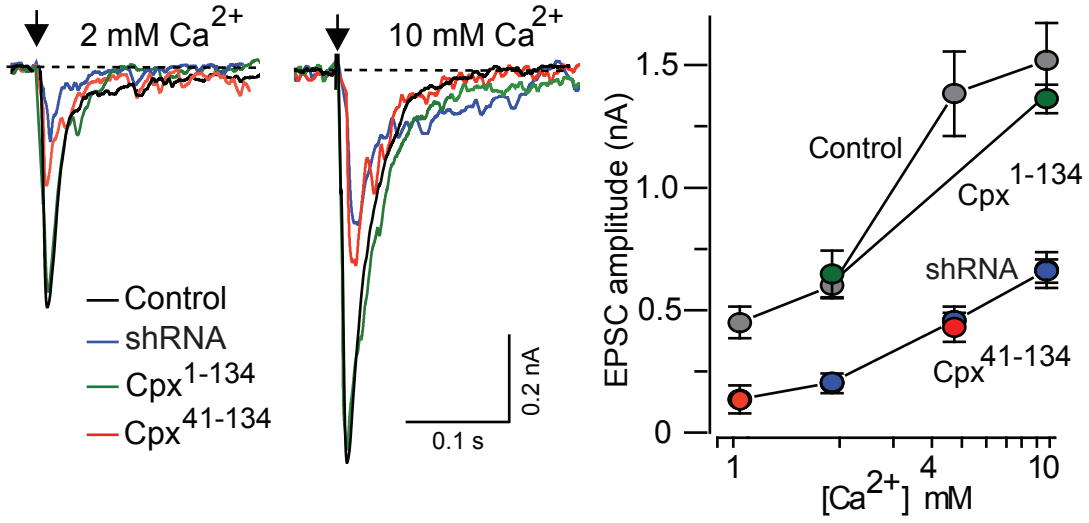

Suppl. Fig. S3
Maximov et al.

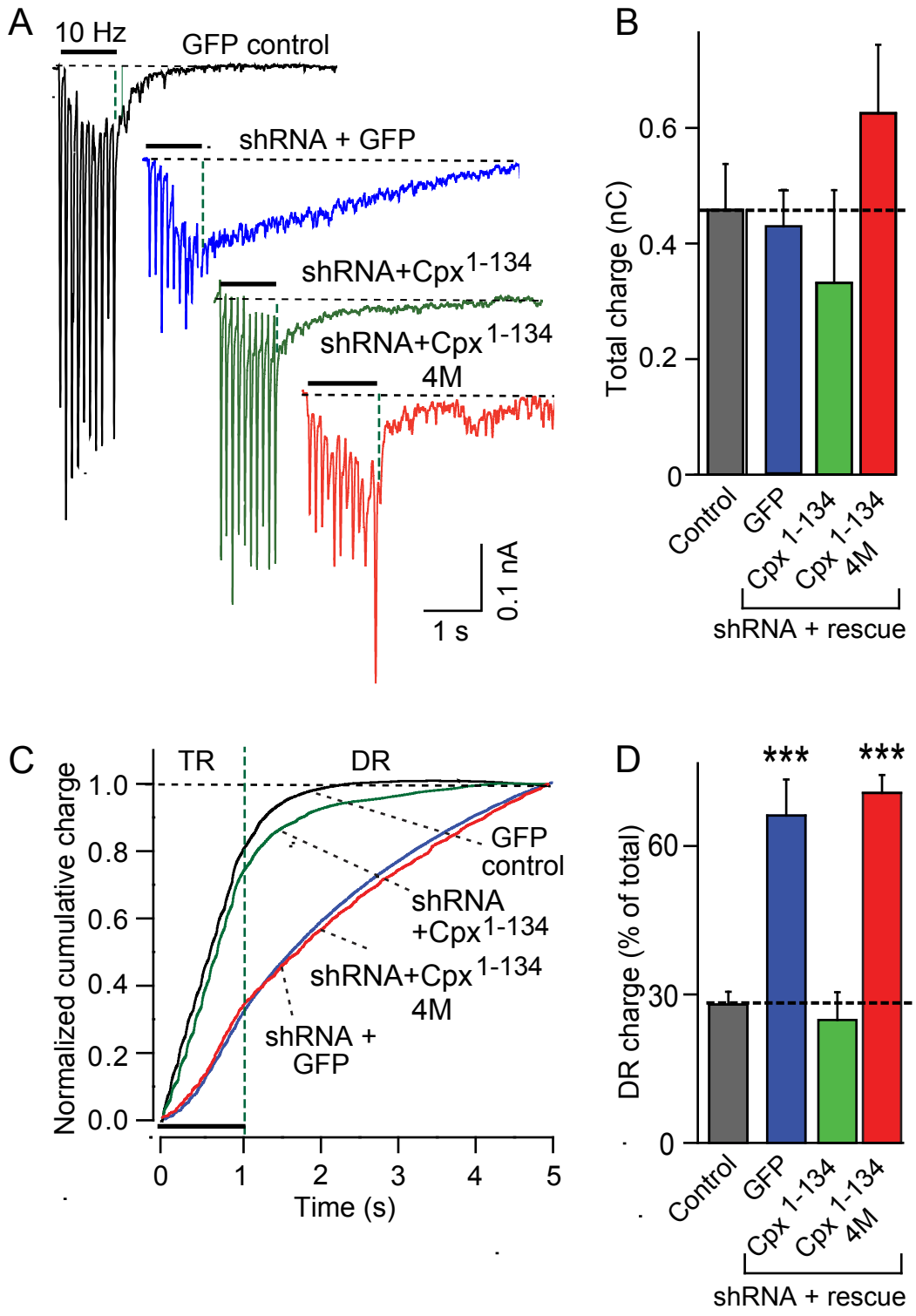

Suppl. Fig. S4
Maximov et al.

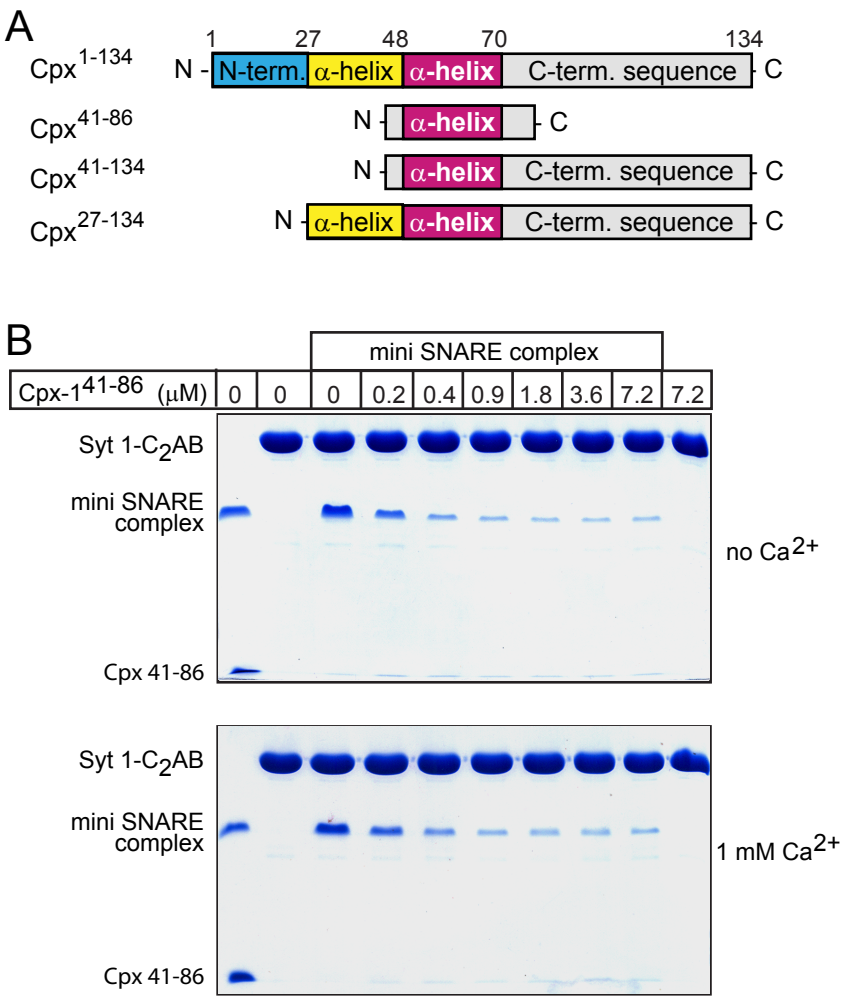

Suppl. Fig. S5
Maximov et al.

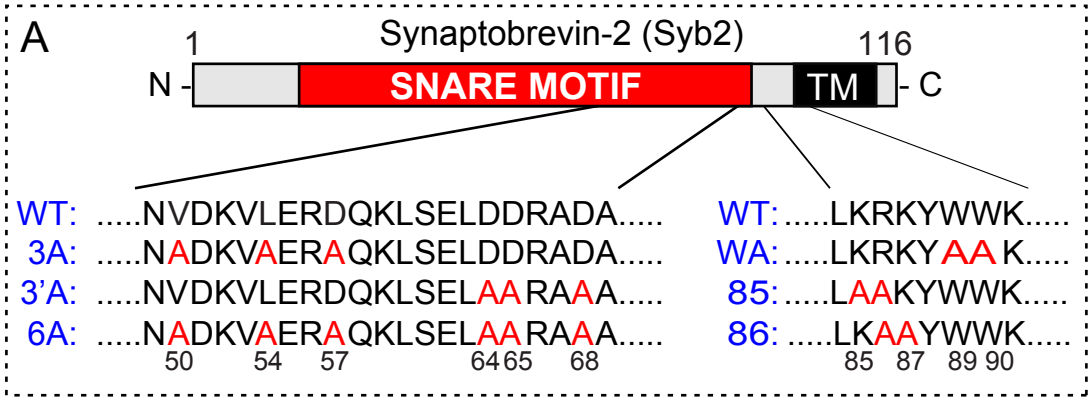

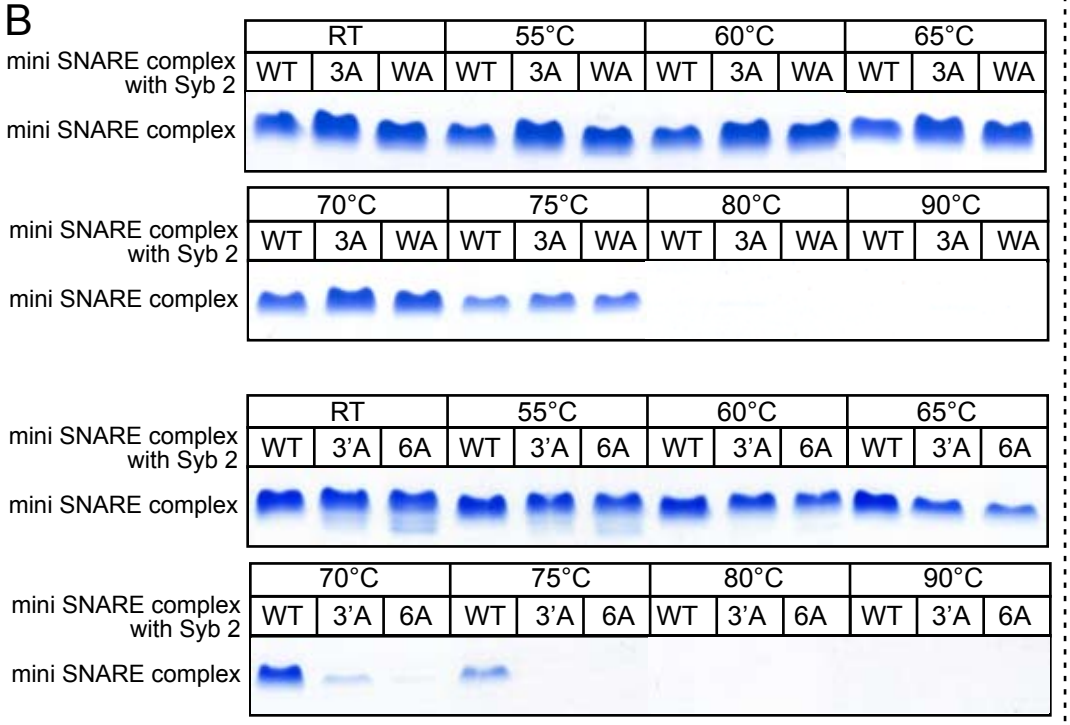

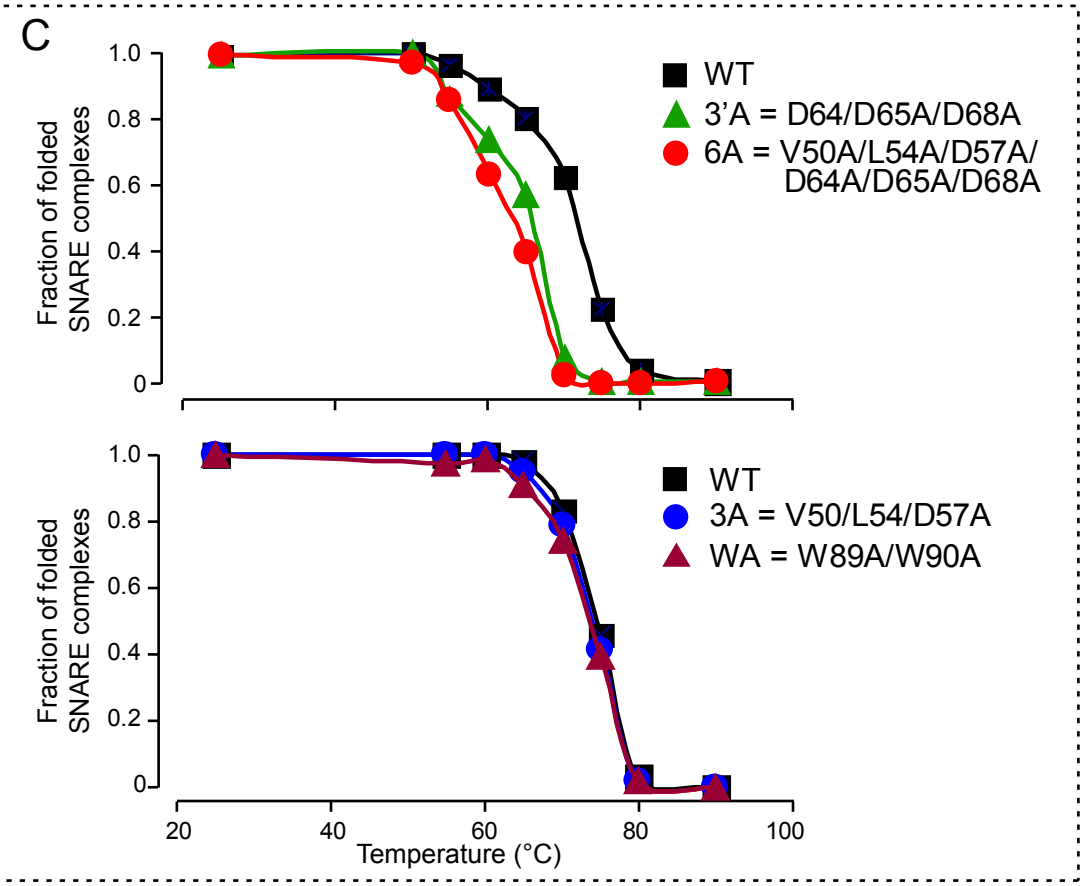

Suppl. Fig. S6
Maximov et al.

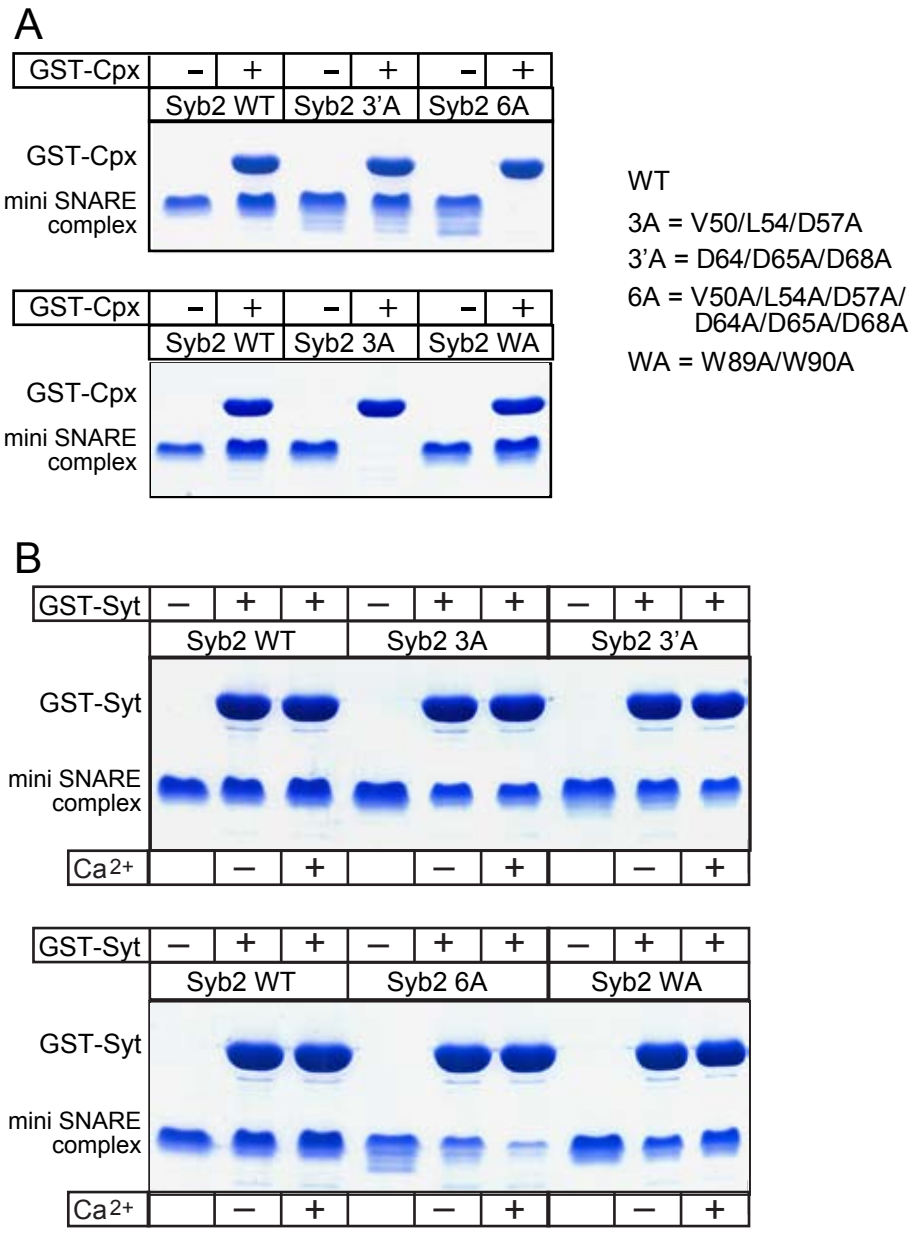

Suppl. Fig. S7
Maximov et al.

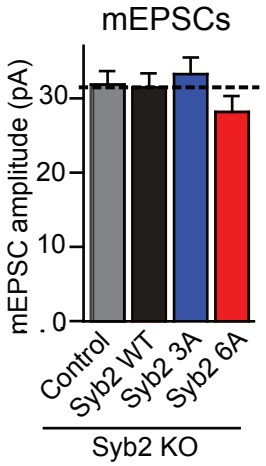

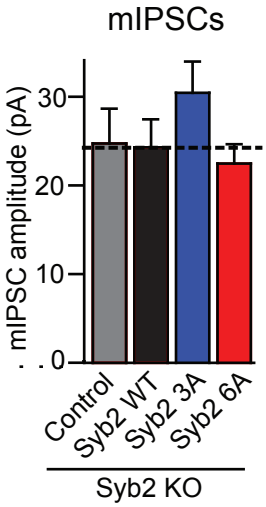

Suppl Fig. S8
Maximov et al.

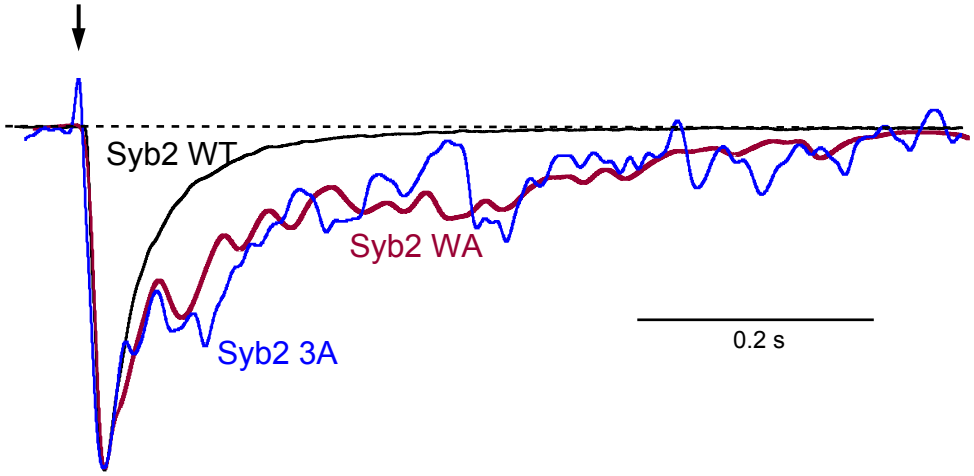

Suppl. Fig. S9
Maximov et al.

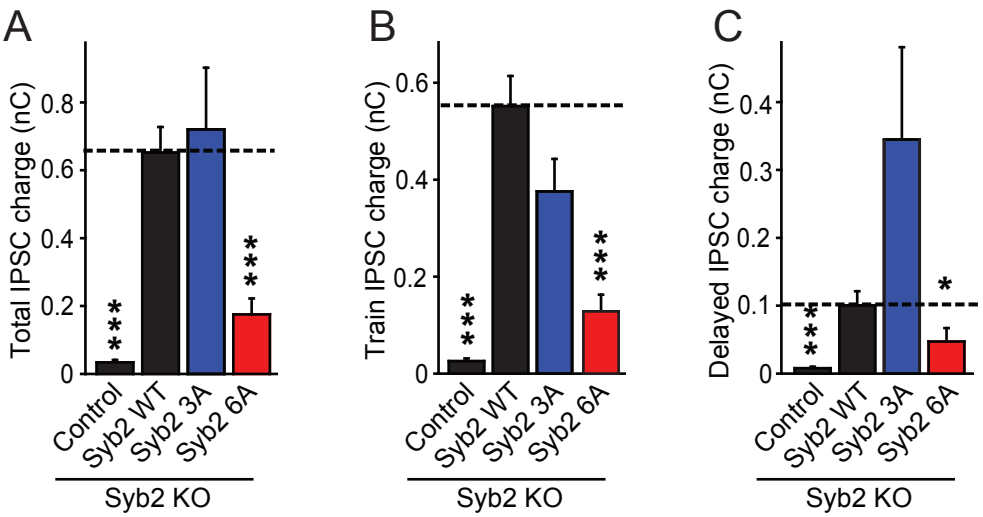

Suppl. Fig. S10
Maximov et al.

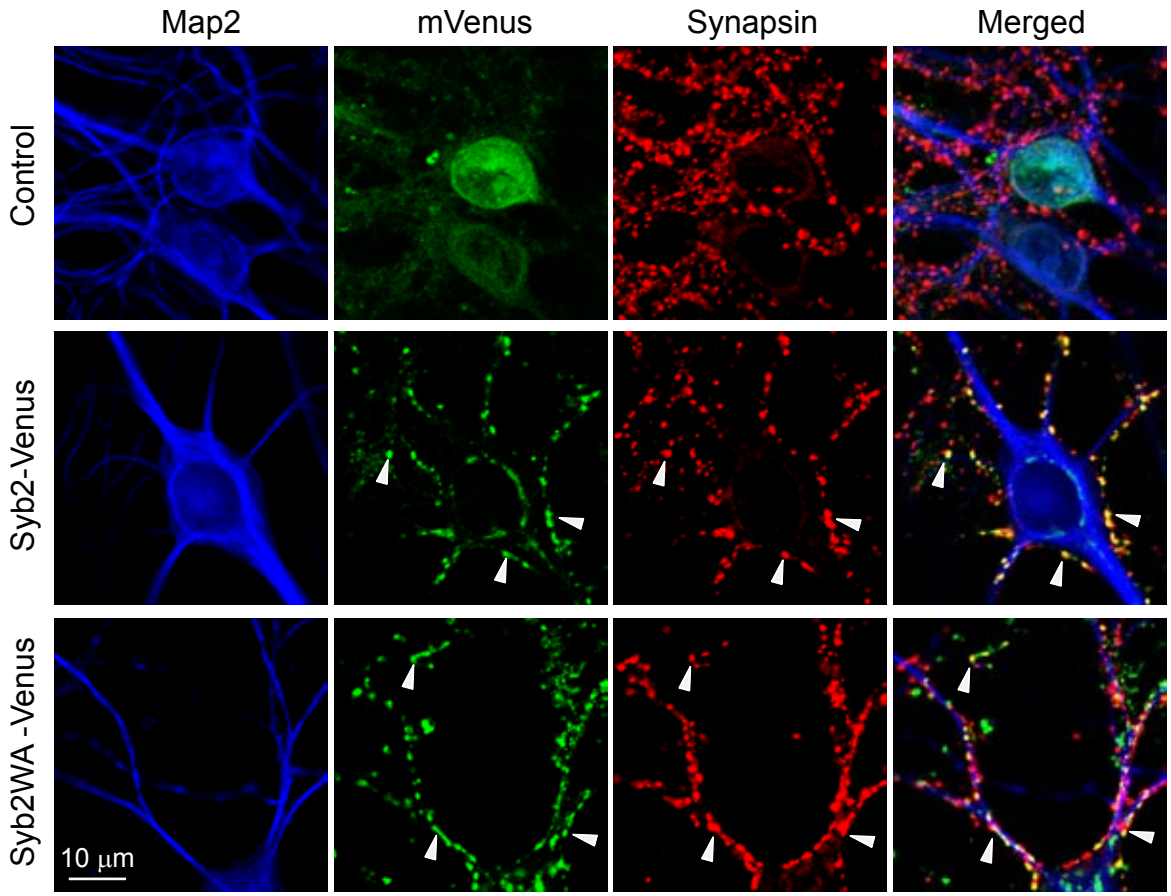

Suppl. Fig. S11
Maximov et al.

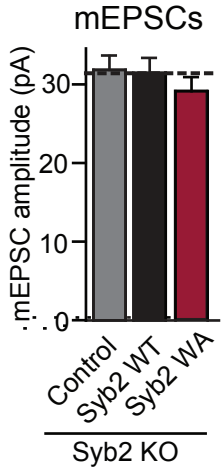

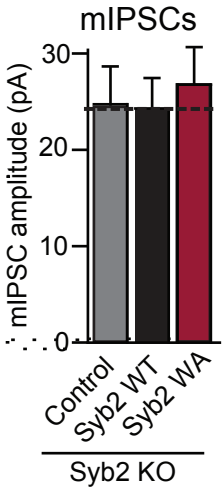

Suppl Fig. S12
Maximov et al.

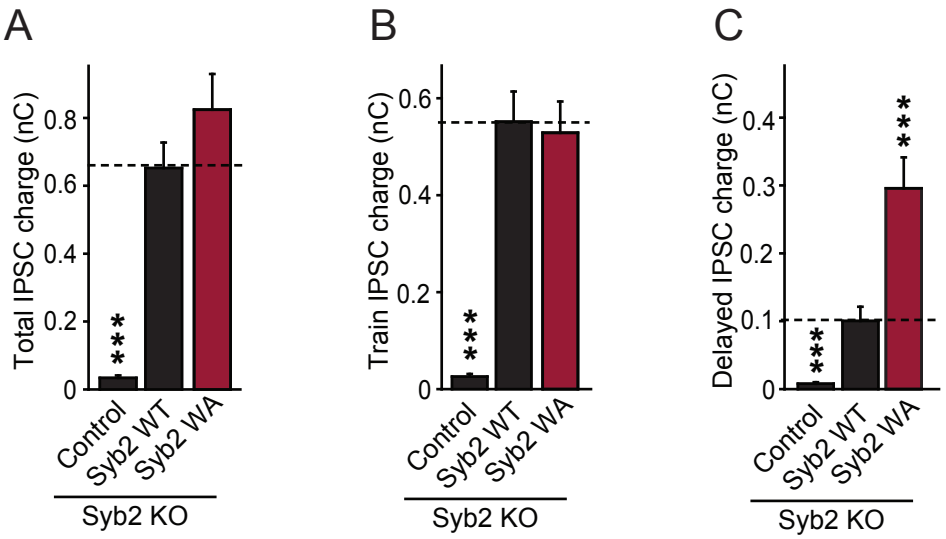

Suppl. Fig. S13
Maximov et al.

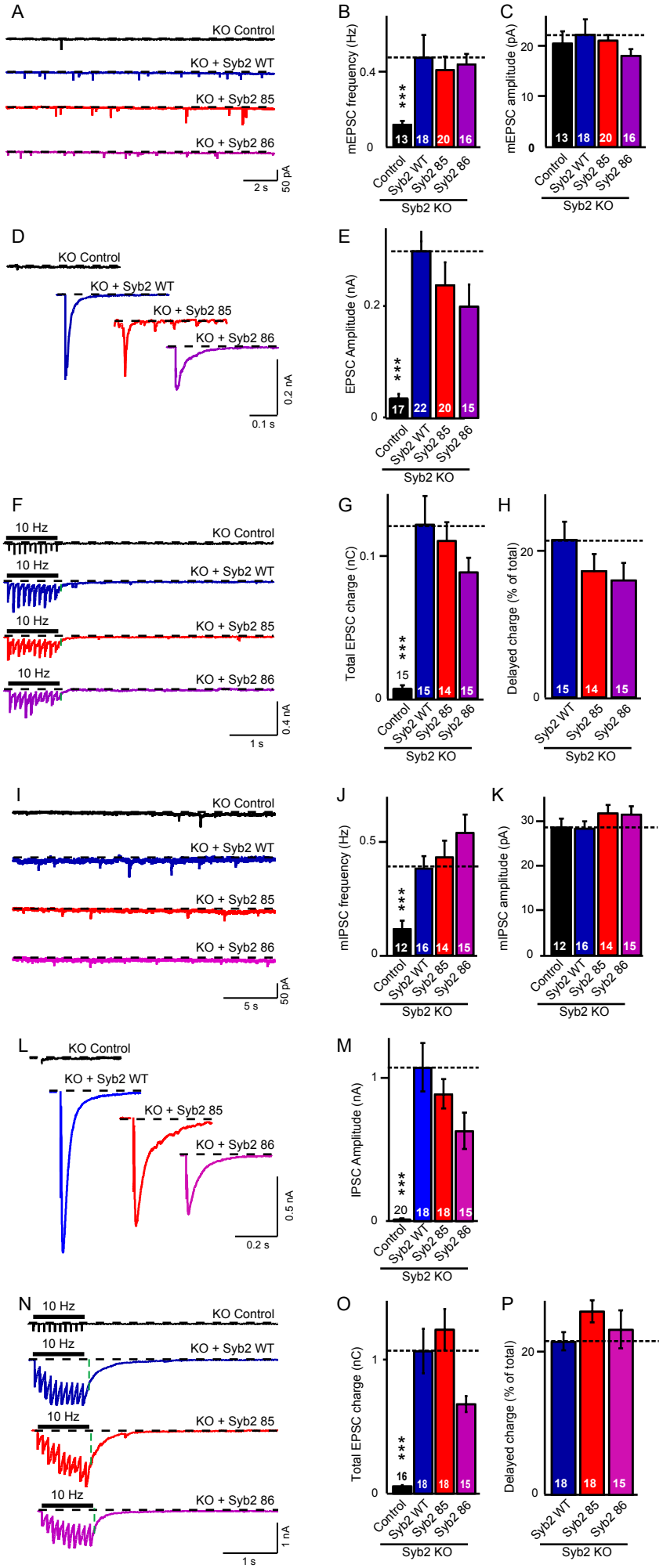

Suppl. Fig. S14
Maximov et al

Supplementary Table 1
Summary of Electrophysiological Data

Figure / Analyzed group	Analyzed parameter (unit) / Value (means±SEMs)	Number of Cultures	Total number of neurons	p Value (ANOVA)
Fig 1A	mEPSC frequency (Hz)			
Control (GFP)	2.3±0.5	6	26	Control
shRNA+GFP	8.8±1.2 (*)	6	33	<0.001
shRNA+Cpx$^{1-134}$	2.1±0.4 (*)	6	23	n.s.
shRNA+Cpx$^{1-134}$ 4M	9.2±1.2	2	13	<0.001
	mEPSC amplitude (pA)			
Control (GFP)	19±1.5	2	12	Control
shRNA+GFP	18±0.8	2	13	n.s.
shRNA+Cpx$^{1-134}$	19±1.8	2	12	n.s.
shRNA+Cpx$^{1-134}$ 4M	21±1.6	2	10	n.s.
Fig 1B	EPSC amplitude (nA)			
Control (GFP)	0.72±0.08	5	20	Control
shRNA+GFP	0.19±0.04	5	22	<0.001
shRNA+Cpx$^{1-134}$	0.68±0.09 (*)	4	17	n.s.
shRNA+Cpx$^{1-134}$ 4M	0.1±0.04	2	10	<0.001
Fig 1D	Normalized mEPSC frequency			
Control (GFP)	1.0±0.1	6	26	Control
shRNA+GFP	4.7±0.38	6	33	<0.001
shRNA+Cpx$^{1-134}$	1.2±0.26	6	23	n.s.
shRNA+Cpx$^{41-86}$	3.8±0.9	1	5	<0.001
shRNA+Cpx$^{41-134}$	2.57±0.3 (*)	6	35	<0.001
shRNA+Cpx$^{27-134}$	0.6±0.1	5	24	n.s.
Fig 1E	Normalized mEPSC amplitude			
Control (GFP)	1.0±0.07	12	44	Control
shRNA+GFP	0.26±0.06	6	19	<0.001
shRNA+Cpx$^{1-134}$	0.97±0.08	5	21	n.s.
shRNA+Cpx$^{41-86}$	0.29±0.06	1	5	<0.001
shRNA+Cpx$^{41-134}$	0.34±0.03	4	19	<0.001
shRNA+Cpx$^{27-134}$	0.43±0.06	5	24	<0.001
---	---	---	---	---
Fig 2B	mEPSC frequency (Hz)			
Control (Syb2 KO)	0.07±0.01	5	31	n.s.
Syb2 WT	0.26±0.05	5	30	Control
Syb2 3A	0.59±0.11	5	22	<0.02
Syb2 6A	0.38±0.06	5	15	n.s.
Fig 2D	mIPSC frequency (Hz)			
Control (Syb2 KO)	0.16±0.04	4	18	<0.05
Syb2 WT	0.59±0.2	4	17	Control
Syb2 3A	1.67±0.3	4	19	<0.001

Syb2 6A	0.59±0.2	4	20	n.s.
Fig 2F	EPSC amplitude (nA)			
Control (Syb2 KO)	0.05±0.01	4	29	<0.001
Syb2 WT	0.18±0.02	4	20	Control
Syb2 3A	0.05±0.01	4	32	<0.001
Syb2 6A	0.03±0.01	4	17	<0.001
	IPSC amplitude (nA)			
Control (Syb2 KO)	0.02±0.001	4	18	<0.001
Syb2 WT	0.72±0.06	4	20	Control
Syb2 3A	0.1±0.02	4	17	<0.001
Syb2 6A	0.08±0.02	4	17	<0.001
Fig 2G	Fast time constant (ms)			
Syb2 WT	40±1	2	10	Control
Syb2 3A	60±5	2	8	<0.001
	Slow time constant (ms)			
Syb2 WT	260±52	2	10	Control
Syb2 3A	812±261	2	8	<0.001
Fig 2I	Total EPSC charge (nC)			
Control (Syb2 KO)	0.03±0.01	4	20	<0.001
Syb2 WT	0.1±0.02	4	18	Control
Syb2 3A	0.06±0.01	4	18	n.s.
Syb2 6A	0.02±0.01	4	14	<0.001
	Total IPSC charge (pC)			
Control (Syb2 KO)	0.03±0.00	4	17	<0.001
Syb2 WT	0.65±0.08	4	21	Control
Syb2 3A	0.58±0.13	4	16	n.s.
Syb2 6A	0.18±0.05	4	16	<0.001
Fig 2J	DR charge, % of total			
Syb2 WT	14±2	4	21	Control
Syb2 3A	32±5	4	16	<0.001
Syb2 6A	20±5	4	16	n.s.
---	---	---	---	---
Fig 3B	mEPSC frequency (Hz)			
Control (Syb2 KO)	0.07±0.01	5	31	n.s.
Syb2 WT	0.26±0.05	5	30	Control
Syb2 WA	0.96±0.2	4	17	<0.02
Fig 3D	mIPSC frequency (Hz)			
Control (Syb2 KO)	0.16±0.04	4	18	<0.05
Syb2 WT	0.59±0.2	4	17	Control
Syb2 WA	1.15±0.1	4	15	<0.02
Fig 3F	EPSC amplitude (nA)			
Control (Syb2 KO)	0.05±0.01	4	29	<0.001
Syb2 WT	0.18±0.02	4	20	Control
Syb2 WA	0.09±0.02	4	17	<0.001

	IPSC amplitude (nA)			
Control (Syb2 KO)	0.02±0.00	4	18	<0.001
Syb2 WT	0.72±0.06	4	20	Control
Syb2 WA	0.38±0.06	4	20	<0.001
Fig 3G	Fast time constant (ms)			
Syb2 WT	40±1	2	10	Control
Syb2 WA	101±18	2	10	<0.001
	Slow time constant (ms)			
Syb2 WT	260±52	2	10	Control
Syb2 WA	742±148 (*)	2	10	<0.001
Fig 3I	Total EPSC charge (pC)			
Control (Syb2 KO)	0.03±0.01	4	20	<0.001
Syb2 WT	0.1±0.02	4	18	Control
Syb2 WA	0.12±0.03 (*)	4	16	n.s.
	Total IPSC charge (pC)			
Control (Syb2 KO)	0.03±0.00	4	17	<0.001
Syb2 WT	0.65±0.08	4	21	Control
Syb2 WA	0.72±1	4	17	n.s.
Fig 3J	DR charge, % of total			
Syb2 WT	14±2	4	21	Control
Syb2 WA	35±2 (*)	4	17	<0.001
---	---	---	---	---
Fig S2B	Synapse density, per 50 μm			
Control (GFP)	24±1	3	36	Control
shRNA+GFP	24±1	3	36	n.s.
	Synapse area (μm^2)			
Control (GFP)	0.58±0.02	3	36	Control
shRNA+GFP	0.57±0.02	3	36	n.s.
Fig S4B	Total charge (nC)			
Control (GFP)	46±8	4	14	Control
shRNA+GFP	42±6	3	12	n.s.
shRNA+Cpx^{1-134}	33±16	2	7	n.s.
shRNA+Cpx^{1-134} 4M	62±12	2	6	n.s.
Fig S4D	Delayed charge, % of total			
Control (GFP)	28±3	4	14	Control
shRNA+GFP	66±7	3	12	<0.001
shRNA+Cpx^{1-134}	25±6	2	7	n.s.
shRNA+Cpx^{1-134} 4M	70±4	2	6	<0.001
Fig S8	mEPSC amplitude (pA)			
Control (Syb2 KO)	32±2	4	20	Control
Syb2 WT	32±2	4	20	n.s.
Syb2 3A	33±2	4	28	n.s.
Syb2 6A	28±2	4	21	n.s.
	mIPSC amplitude (pA)			
Control (Syb2 KO)	24±4	2	5	Control

Syb2 WT	24±3	2	5	n.s.
Syb2 3A	31±3	2	6	n.s.
Syb2 6A	22±2	2	6	n.s.
Fig S10A	Total IPSC charge (nC)			
Control (Syb2 KO)	0.03±0.00	4	17	<0.001
Syb2 WT	0.65±0.08	4	21	Control
Syb2 3A	0.72±0.18	4	16	n.s.
Syb2 6A	0.18±0.05	4	16	<0.001
Fig S10B	Train IPSC charge (nC)			
Control (Syb2 KO)	0.02±0.00	4	17	<0.001
Syb2 WT	0.55±0.06	4	21	Control
Syb2 3A	0.38±0.07	4	16	n.s.
Syb2 6A	0.13±0.04	4	16	<0.001
Fig S10C	Delayed IPSC charge (nC)			
Control (Syb2 KO)	0.01±0.00	4	17	<0.001
Syb2 WT	0.1±0.02	4	21	Control
Syb2 3A	0.34±0.18	4	16	n.s.
Syb2 6A	0.04±0.02	4	16	<0.05
Fig S12	mEPSC amplitude (pA)			
Control (Syb2 KO)	32±2	4	20	n.s.
Syb2 WT	32±2	4	20	Control
Syb2 WA	29±2	4	20	n.s.
	mIPSC amplitude (pA)			
Control (Syb2 KO)	24±4	2	6	n.s.
Syb2 WT	24±3	2	6	Control
Syb2 WA	26±4	2	6	n.s.
Fig S13A	Total IPSC charge (nC)			
Control (Syb2 KO)	0.03±0.00	4	17	<0.001
Syb2 WT	0.65±0.08	4	21	Control
Syb2 WA	0.82±0.1	3	17	n.s.
Fig S13B	Train IPSC charge (nC)			
Control (Syb2 KO)	0.02±0.00	4	17	<0.001
Syb2 WT	0.55±0.06	4	21	Control
Syb2 WA	0.53±0.06	4	17	n.s.
Fig S13C	Delayed IPSC charge (nC)			
Control (Syb2 KO)	0.08±0.00	4	17	<0.001
Syb2 WT	0.1±0.08	4	21	Control
Syb2 WA	0.3±0.03	4	17	<0.001
Fig S14B	mEPSC frequency (Hz)			
Control (Syb2 KO)	0.12±0.02	4	13	<0.001
Syb2 WT	0.48±0.1	4	18	Control
Syb2 85	0.42±0.07	4	20	n.s.
Syb2 86	0.45±0.05	3	16	n.s.
Fig S14C	mEPSC amplitude (pA)			
Control (Syb2 KO)	21±2	4	13	n.s.

Syb2 WT	23±3	4	18	Control
Syb2 85	21±1	4	20	n.s.
Syb2 86	18±1	3	16	n.s.
Fig S14E	EPSC amplitude (nA)			
Control (Syb2 KO)	0.03±0.00	4	17	<0.001
Syb2 WT	0.29±0.03	4	22	Control
Syb2 85	0.23±0.04	4	20	n.s.
Syb2 86	0.19±0.04	3	15	n.s.
Fig S14G	Total EPSC charge (nC)			
Control (Syb2 KO)	0.01±0.00	4	15	<0.001
Syb2 WT	0.12±0.02	4	15	Control
Syb2 85	0.11±0.01	4	14	n.s.
Syb2 86	0.09±0.01	3	15	n.s.
Fig S14H	Delayed EPSC charge, % of total			
Syb2 WT	22±2	4	15	Control
Syb2 85	18±2	4	14	n.s.
Syb2 86	16±2	3	15	n.s.
Fig S14J	mIPSC frequency (Hz)			
Control (Syb2 KO)	0.11±0.03	4	12	<0.001
Syb2 WT	0.39±0.05	4	16	Control
Syb2 85	0.44±0.07	4	14	n.s.
Syb2 86	0.55±0.08	3	15	n.s.
Fig S14K	mIPSC amplitude (pA)			
Control (Syb2 KO)	29±2	4	12	n.s.
Syb2 WT	29±2	4	16	Control
Syb2 85	32±2	4	14	n.s.
Syb2 86	32±2	3	15	n.s.
Fig S14M	IPSC amplitude (nA)			
Control (Syb2 KO)	0.02±0.00	4	20	<0.001
Syb2 WT	1.09±0.17	4	18	Control
Syb2 85	0.90±0.10	4	18	n.s.
Syb2 86	0.72±0.12	3	15	n.s.
Fig S14O	Total IPSC charge (nC)			
Control (Syb2 KO)	0.06±0.01	4	16	<0.001
Syb2 WT	1.07±0.17	4	18	Control
Syb2 85	1.24±0.15	4	18	n.s.
Syb2 86	0.68±0.06	3	15	n.s.
Fig S14P	Delayed IPSC charge, % of total			
Syb2 WT	22±1	4	18	Control
Syb2 85	26±2	4	18	n.s.
Syb2 86	21±2	3	15	n.s.

(*) = Additional data points were added after figures were finalized, but only the precise number changes.

n.s. = Not significant

SUPPLEMENTARY REFERENCES

S1. A. Maximov, Z.P. Pang, D.G. Tervo, T.C. Südhof *J. Neurosci. Methods* **161**, 75 (2007)

S2. J. Xu, T. Mashimo, T.C. Sudhof. *Neuron* **54**, 567 (2007)

S3. S. Schoch *et al., Science* **294**, 1117 (2001)

S4. C. Lois, E.J. Hong, S. Pease, E.J. Brown, D. Baltimore. *Science* **295**, 868 (2002)

S5. H.T. McMahon, M. Missler, C. Li, T.C. Südhof. *Cell* **83**, 111 (1995).

S6. J. Tang et al., *Cell* **126**, 1175 (2006)

S7. X. Chen *et al.,* Neuron ***33*,** 397 (2002).

S8. Z.P. Pang, J. Sun, J. Rizo, A. Maximov, T.C. Südhof. *EMBO J. **25,*** 2039 (2006)

S9. A. Maximov, T.C. Südhof *Neuron* **48,** 547 (2005).

S10. K. Reim *et al., Cell* **104,** 71 (2001).

S11. M. Xue *et al., Nat. Struct. Mol .Biol. **14,*** 949 (2007).

S12. M. Geppert *et al., Cell* **79,** 717 (1994).

S13. C.G. Giraudo, W.S. Eng, T.J. Melia, J.E. Rothman. *Science* **313,** 676 (2006).

S14. C. G. Giraudo *et al., J. Biol. Chem.* **283,** 21211 (2008)

S15. S. Huntwork, J.T. Littleton. *Nat. Neurosci.* **10,** 1235(2007).

S16. T.C. Südhof. *Annu. Rev. Neurosci.* **27**, 509 (2004).

S17. V. Budnik. *Curr. Opin. Neurobiol.* **6,** 858 (1996).

S18. F. Deák, E.T. Kavalali, T.C. Südhof. *J. Neurosci.* **26**, 6668 (2006).

S19. J. Kesavan, M. Borisovska, D. Bruns. *Cell* **131,** 351 (2007).